Journal of Nuclear Materials 629 (2026) 156680

Contents lists available at ScienceDirect

Journal of Nuclear Materials

journal homepage: www.elsevier.com/locate/jnucmat

Thermodynamic properties of uranium-zirconium carbide solid solutions with oxygen

Gustavo Costa [a,*], Malina K. Slizik [a], Jason C. Reynolds [b], Scarlett Widgeon Paisner [c], Joseph C. Schaeperkoetter [c], Erofili Kardoulaki [c], Shinhyo Bang [d], Xiaofeng Guo [d], Theodore M. Besmann [e]

[a] NASA Glenn Research Center, 21000 Brookpark Road, Cleveland, OH 44135, USA
[b] NASA Marshall Space Flight Center, 21000 Brookpark Road, Cleveland, OH 44135, USA
[c] Los Alamos National Laboratory, P.O. Box 1663, Los Alamos, NM 87545, USA
[d] Department of Chemistry, Washington State University, Pullman, WA 99164, USA
[e] General Atomics SmartState Center for Transformational Nuclear Technologies, University of South Carolina, Columbia, SC 29208, USA

ARTICLE INFO

Keywords:
Uranium-zirconium carbide
Nuclear fuels
Space reactors
Thermodynamics
Calorimetry

ABSTRACT

Uranium-zirconium carbide solid solutions are potential candidates for fuel in space nuclear reactors. To support development of advanced robust fuels for space applications, $(U_yZr_{1-y})C_xO_z$ solid solutions were synthesized via carbothermic reduction with uranium, carbon, and oxygen contents raging from y = 0.05 – 0.3, x = 0.95 – 0.98, and z = 0.02 – 0.07. These solid solutions were subsequently characterized by X-ray diffraction and elemental combustion analysis. High-temperature oxidative drop solution calorimetry in molten sodium molybdate solvent at 1073 K was employed to determine the formation, oxidation, and mixing enthalpies of $(U_yZr_{1-y})C_xO_z$ solid solutions, and thereby for evaluating their thermodynamic stability. The solid solutions are enthalpically less stable than the UC and ZrC end members. They also become less stable and more reactive towards oxidation with increasing uranium content. Incorporation of oxygen into solid solutions increases their solid solution-stability and improves their oxidation resistance.

1. Introduction

The growing demand for space and planetary exploration has renewed interest in advanced propulsion and power systems based on nuclear energy. Building on the legacy of the Rover and Nuclear Engine for Rocket Vehicle Application (NERVA) programs conducted from 1950s to the early 1970s, NASA has reinitiated the development of nuclear propulsion technologies. The current Space Nuclear Propulsion (SNP) program is focused on nuclear thermal propulsion (NTP) systems employing high-assay low-enriched uranium (HALEU) fuel. HALEU, containing 10–20 Wt.% ^{235}U, is capable of operation at temperatures exceeding 2700 K, enabling specific impulses greater than 900 s, which are substantially higher than those achievable with chemical propulsion systems (450 s) and is therefore well suited for interplanetary missions such as Mars and the Jovian system [1].

Uranium-zirconium carbide, $(U_yZr_{1-y})C_x$, solid solutions have been widely investigated as candidate fuels for NTP and nuclear power applications [2–7]. Interest in this material system stems from its favorable thermophysical and chemical properties, including high melting temperature, adequate thermal conductivity, and compatibility with hydrogen environments [5,8–10]. Prior studies have examined hydrogen compatibility, thermophysical behavior, and phase equilibria within U-Zr-C ternary system across selected composition ranges to improve the high-temperature stability of uranium carbide phases and optimize fuel performance [2,4,6,7,9–11].

Phase equilibria and thermodynamic properties of selected U-Zr-C compositions were investigated at Los Alamos National Laboratory (LANL) to identify approaches for enhancing uranium stability in carbide phases and improving key fuel characteristics such as melting temperature, oxidation resistance, and high-temperature mechanical strength [4,6]. These efforts included measurements of uranium and zirconium thermodynamic activities in $(U_yZr_{1-y})C_x + C_{(graphite)}$ and $(U_yZr_{1-y})C_x + UC_2 + C_{(graphite)}$ systems between 1749 and 2437 K using Knudsen effusion mass spectrometry (KEMS) [4]. The resulting activity

* Corresponding author.
E-mail address: gustavo.costa@nasa.gov (G. Costa).

https://doi.org/10.1016/j.jnucmat.2026.156680
Received 1 December 2025; Received in revised form 14 April 2026; Accepted 19 April 2026
Available online 19 April 2026
0022-3115/Published by Elsevier B.V.

data were used to calculate solid solution mixing Gibbs free energies and enthalpies. The mixing enthalpy was found to be zero at 2190 K and positive at higher temperatures, indicating increasing solid solution thermodynamic instability with increasing temperature. Phase boundary measurements further showed that the equilibrium between $(U_yZr_{1-y})C_x$, UC_2, and $C_{(graphite)}$ shifts toward lower uranium contents with increasing temperature.

In parallel, LANL developed $(U_yZr_{1-y})C_x$ solid solutions with hypostoichiometric carbon as alternatives to the pyrocarbon-coated UC_2 fuel kernels used in earlier NTP reactors [2]. For the $U_{0.1}Zr_{0.9}C_x$ system, stable operation near the melting temperature was shown to require carbon contents between x = 0.88 and 0.95. Thermochemical equilibrium calculations using Thermo-Calc (version 2025a) [12] with the Thermodynamics of Advanced Fuels – International Database (TAF-ID) [13] indicates maximum melting temperature of approximately 3087 K at x = 0.94 as shown in the recalculated $(U_{0.1}Zr_{0.9})C_x$ pseudobinary phase diagram in Fig. 1. Fuel elements fabricated from $U_{0.1}Zr_{0.9}C_{0.9}$ were successfully tested in the Nuclear Furnace – 1 reactor at LANL, demonstrating acceptable performance under hydrogen at temperatures up to 2800 K for extended operation times.

Subsequent optimization of the U-Zr-C phase diagram between 2473 and 3693 K identified single-phase $(U_yZr_{1-y})C_x$ compositions and narrow two-phase regions with carbon as the most promising operating regimes for high-temperature NTP applications [7]. Increasing temperature was shown to favor lower uranium contents, with single-phase region shifting toward Zr-rich compositions. Single-phase solid solutions were determined to offer greater performance potential than two-phase materials at elevated temperatures.

More recently, joint NASA-LANL efforts have focused on targeted $(U_yZr_{1-y})C_x$ solid solution compositions with hypostoichiometric carbon for NTP applications [10,11,14]. These studies reported the syntheses, thermophysical characterization, and hot hydrogen compatibility testing of compositions with uranium contents of y = 0.05 – 0.3 and carbon contents of x = 0.8 – 0.95. Notably, $U_{0.2}Zr_{0.8}C_{0.93}$ exhibited increasing thermal conductivity with temperature and minimal mass loss during high-temperature hydrogen exposure, with no evidence of significant cracking or phase degradation. Although these investigations established promising chemical and thermophysical performance, comprehensive chemical thermodynamic data remains limited.

A comprehensive understanding of the thermodynamic properties of uranium–zirconium carbide (U,Zr)C systems, including those materials containing oxygen, is essential for advancing their use in high temperature nuclear applications, particularly in NTP technologies. Oxygen is an unavoidable impurity introduced during the synthesis and processing of carbides, where high surface area powders, carbothermal reduction routes, and high temperature homogenization steps increase exposure to oxidizing species. As noted by Ang [15], oxygen acts as a pervasive impurity in ZrC and is expected to affect processing of (U,Zr)C as well, which underscores its direct influence on phase stability, carbon thermodynamic activity, and microstructural evolution. Oxygen contamination can shift solidus boundaries, promote secondary phase formation, and alter melting behavior, all of which are critical for fuels designed to operate between 2000–3000 K. For example, a recent work on U-C-O system confirmed the possible formation of metastable U $(C_{1-x}O_x)_2$ secondary phase [16]. Thus, understanding how oxygen modifies the thermodynamic landscape of (U,Zr)C is therefore essential for accurate fuel performance modeling, predicting degradation pathways, and designing robust carbide fuels for next generation aerospace nuclear systems.

In the present study, oxidative drop solution calorimetry was used to determine the enthalpies of formation, mixing, and oxidation of $(U_yZr_{1-y})C_xO_z$ solid solutions with uranium, carbon, and oxygen contents of y = 0.05 – 0.3, x = 0.95 – 0.98, and z = 0.02 – 0.07, respectively. Trends in enthalpic stability as a function of uranium content and the influence of oxygen on solid solution energetics are examined. The thermodynamic data generated in this work are essential for incorporation into CALPHAD based databases [13] used in fuel thermochemical modeling and for assessing its stability in NTP reactor environments.

2. Materials and methods

2.1. Materials

2.1.1. Solid-solutions

Powder $(U_yZr_{1-y})C_xO_z$ solid-solution feedstocks were synthesized by the carbothermic reduction (CTR) method as described in detail in

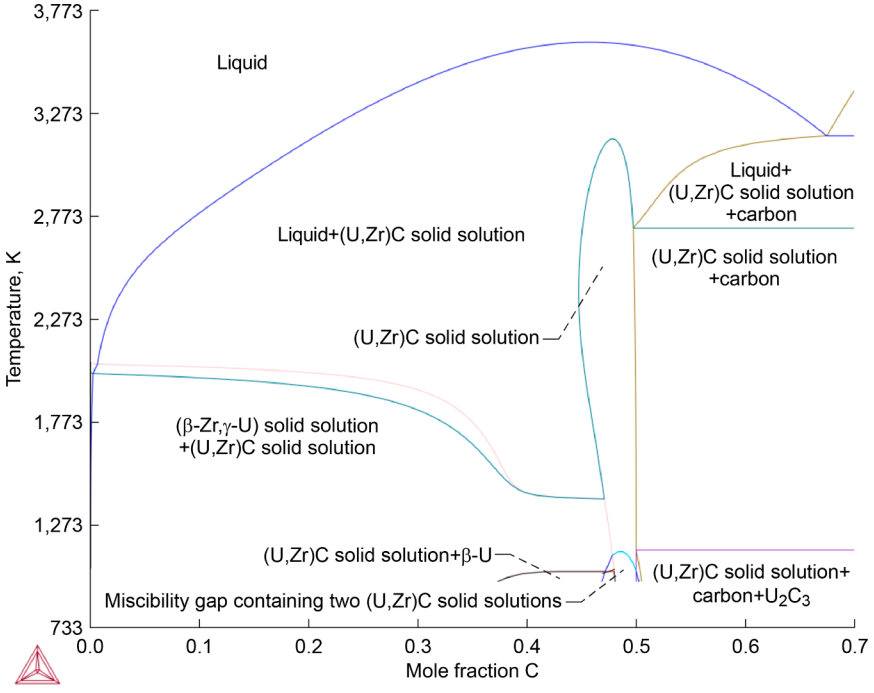

Fig. 1. Calculated pseudo-binary phase diagram of the $(U_{0.1}Zr_{0.9})C_x$ solid solution.

Kardoulaki et al. [10]. The samples were prepared by mixing uranium oxide ($UO_{2.16}$, Framatome) with zirconium oxide (ZrO_2, Alfa Aesar, 99.7%) and graphite ($C_{graphite}$, Alfa Aesar, 99.9995%) to produce $(U_yZr_{1-y})C_xO_z$ samples with chemical compositions of varied uranium (y = 0.05, 0.1, 0.2, and 0.3) and fixed carbon (x = 0.95) contents. The precursor powder samples were homogenized in a SPEX Centriprep high-energy mill for 30 min. The precursors were then pressed into pellets and heat treated at 2073 K. The resulting pellets were ground in a tungsten carbide mortar and sieved to produce the powder samples that were sent to NASA Marshall Space Flight Center for direct-current sintering following a previously described procedure [11]. All processing steps were conducted within an argon glove box.

2.1.2. End-member and reference materials

ZrC (99.5% pure) powdered sample was purchased from Alfa Aesar. Further details about ZrC sample are described in the supporting information.

UO_2 powdered sample was synthesized by precipitation from a uranyl nitrate solution purchased from International Bio-Analytical Industries, Inc. Further details about UO_2 synthesis are described in the supporting information.

2.2. Sample structural and chemical characterization

Atomic concentrations of carbon and oxygen were determined through elemental combustion analysis coupled with infrared absorption using LECO C844 and LECO ONH836 analyzers (LECO corporation, Michigan, USA) for carbon and oxygen, respectively. Each sample was measured in triplicate using approximately 0.1 g of material, then either placed in an alumina crucible with tin and copper accelerant for carbon analysis or placed in a graphite crucible with tin and zinc accelerants for oxygen analysis. The ratio of uranium to zirconium is assumed to be consistent with the batched ratio from CTR, and the full quantified composition is calculated with the assumption of 100% occupancy of the U/Zr site.

XRD patterns for powder $(U_yZr_{1-y})C_xO_z$ and ZrC samples were gathered in a D8 Advance diffractometer (Bruker-AXS GmbH, Karlsruhe, Germany) from 10° to 90° 2θ with a step size of 0.020° and a collection time of 2.5 s/step. Samples were placed on zero-diffraction Si discs and then mounted in airtight specimen holders in an argon glove box prior to the analysis. Phase identification, whole pattern fitting, and Rietveld refinement were carried out to calculate the lattice parameters using Jade 2010 v.3 software (Materials Data, Inc., Livermore, CA) with the International Centre for Diffraction Data (ICDD) Powder Diffraction File (PDF-4+, 2019).

2.3. High-temperature oxidative drop solution calorimetry

High-temperature oxidative drop solution calorimetry was carried out in an AlexSys Setaram isoperibol Tian-Calvet twin microcalorimeter (Caluire-et-Cuire, Auvergne-Rhône-Alpes, France). This is a well-established technique to measure the integral thermodynamic properties of a wide variety of materials, including uranium-based carbides [17–20]. Approximately 5 mg of powdered $(U_yZr_{1-y})C_xO_z$ samples were weighed and pressed in a steel die in an argon glovebox containing 0.46 ppm O_2 and 0.02 ppm H_2O to produce compacted powder samples for calorimetric experiments. The new, custom airtight sample dispenser shown in Fig. 2 was used to transfer and drop the samples into the calorimeter without exposure to air. This is accomplished in four steps. Step 1: The sample (white) was placed in the vial (gray) and weighed with the tared dispenser (red). Step 2: The magnet (dark gray) and cap (black) were placed on the top of the vial. Step 3: The assembled dispenser containing the sample was removed from the glove box and placed on the calorimeter dropping tube and the metallic pin (dark gray) was removed from the vial. Step 4: The magnet was removed from the cap to open the trap door, releasing the sample in the calorimeter (Fig. 3). Each of the two calorimeter glassware assemblies (Fig. 3) contained Pt crucibles loaded with 20 g of sodium molybdate ($3Na_2O$-$4MoO_3$). The calorimeter assembly was purged with oxygen at 22.1 mL/min, and the solvent was bubbled with oxygen at 2.3 mL/min to aid dissolution and complete oxidation of the samples. Measurements were carried out at 1073 K and repeated 6 to 8 times to achieve statistically reliable data. The calorimeter was calibrated using high-purity platinum metal specimens. The measured drop solution enthalpy (ΔH_{ds}) includes the heat content of the sample from room temperature to 1073 K (ΔH_{TTD}) plus the solution enthalpy (ΔH_{sol}) of the sample in the solvent.

2.4. Thermochemical computational methods

Uranium, zirconium, and carbon oxidation enthalpies at 298 K, and O_2 and CO_2 sensible enthalpies from 298 K to 1073 K required in the thermochemical calculations of the $(U_yZr_{1-y})C_xO_z$ oxidation and formation enthalpies were computed using the reaction module of FactSage software 8.3 [21] integrated with FactPS database, which contains data from [22–24]. For comparison purposes with calorimetric experimental data, ZrC formation enthalpy was also computed using the same computational methodology described in the prior sentence Table 3.

3. Results

The chemical composition of the samples (Table 1) was used to calculate the stoichiometric coefficients shown in Table 2. The stoichiometric coefficients were used in the thermochemical cycles to

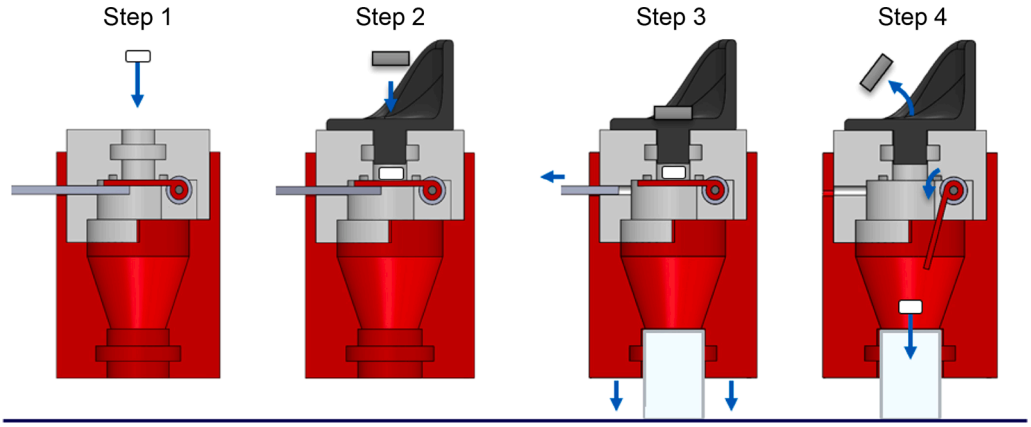

Fig. 2. Graphical representation of the drop calorimeter airtight sample dispenser and steps of the experiment.

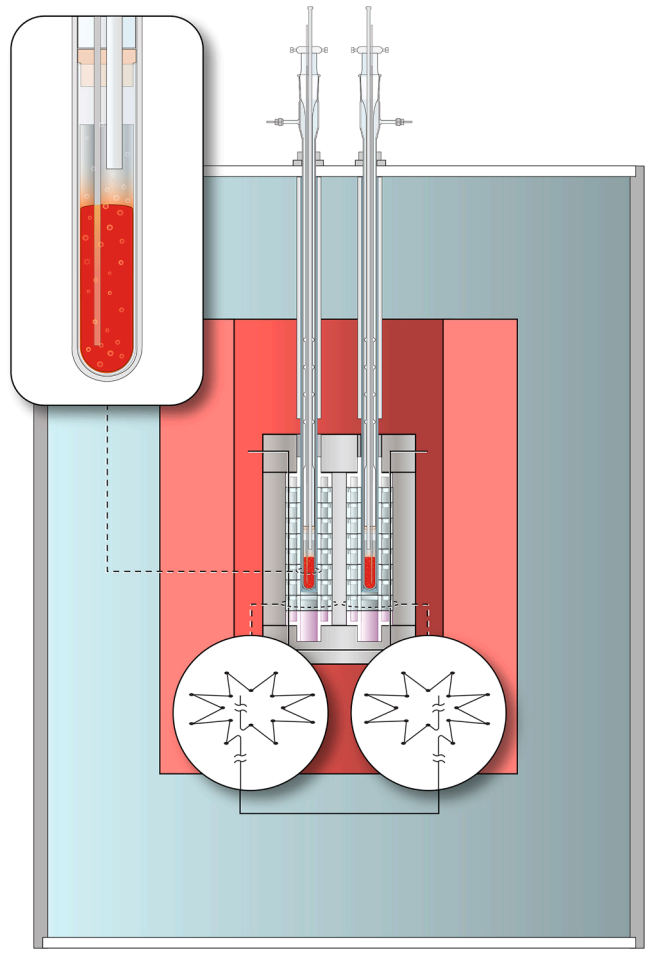

Fig. 3. Graphical representation of the drop solution calorimeter.

Table 1
Chemical composition of the $(U_yZr_{1-y})C_xO_z$ phase measured by elemental combustion analysis and XRD.

Sample ID	Content (at.%)			
	U	Zr	C	O
$U_{0.05}Zr_{0.95}C_{0.95}O_{0.024}$	2.54	48.22	48.02	1.22
$U_{0.1}Zr_{0.9}C_{0.95}O_{0.030}$	5.06	45.53	47.91	1.50
$U_{0.2}Zr_{0.8}C_{0.96}O_{0.026}$	10.09	40.36	48.25	1.30
$U_{0.3}Zr_{0.7}C_{0.98}O_{0.068}$	14.57	34.22	47.90	3.31

Table 2
Calculated stoichiometric coefficients of each studied sample formula. Coefficients are normalized to 100% occupancy of the U/Zr site.

Sample ID	$(U_yZr_{1-y})C_xO_z$ Stoichiometric Coefficients*			
	y	1 – y	x	z
$U_{0.05}Zr_{0.95}C_{0.95}O_{0.024}$	0.0500 ±0.0003	0.950 ±0.005	0.946 ±0.005	0.0240 ±0.0001
$U_{0.1}Zr_{0.9}C_{0.95}O_{0.030}$	0.1000 ±0.0005	0.900 ±0.005	0.947 ±0.005	0.0300 ±0.002
$U_{0.2}Zr_{0.8}C_{0.96}O_{0.026}$	0.200 ±0.001	0.800 ±0.004	0.956 ±0.005	0.0260 ±0.0001
$U_{0.3}Zr_{0.7}C_{0.98}O_{0.068}$	0.299 ±0.002	0.701 ±0.004	0.982 ±0.005	0.0680 ±0.0003

*Uncertainties are assumed to be 0.5% error in the coefficients.

calculate the formation, oxidation, and mixing enthalpies of the samples.

The XRD patterns of the $(U_yZr_{1-y})C_xO_z$ solid solution samples are presented in Fig. 4. Only cubic phase (space group $Fm\bar{3}m$) was detected in the samples synthesized by the carbothermic reduction method, except for the $U_{0.3}Zr_{0.7}C_{0.98}O_{0.068}$ sample which had 0.83 wt.% cubic UO_2. The unit-cell parameters and volume of the samples, obtained from whole-pattern fitting and Rietveld refinement, are given in Table 3; the measured unit cell parameters are consistent with those previously reported [11]. Fig. 5 shows the unit cell parameters of the $(U_yZr_{1-y})C_xO_z$ samples as a function of uranium content where parameter a is seen to decrease linearly with uranium content, consistent with Vegard's law. All datapoints of the samples in Fig. 5, except for $U_{0.3}Zr_{0.7}C_{0.98}O_{0.068}$, were fitted using Eq. (1):

$$a = (4.6949\pm0.0007) + (0.270\pm0.004)\, y\,. \quad (1)$$

in which the adjusted coefficient of determination $R^2 = 0.9993$.

The measured drop solution enthalpies (ΔH_{ds}) of the $(U_yZr_{1-y})C_xO_z$ and ZrC samples, along with reported values for ZrO_2 and UO_3 [25,26], are shown in Table 4. $U_{0.3}Zr_{0.7}C_{0.98}O_{0.068}$ drop solution enthalpy was corrected assuming the energetic contribution of the UO_2 phase, with details provided in the supporting information. The ΔH_{ds} of UC, also reported in Table 4, was calculated from that measured by Goncharov et al. [17] at 973 K, but was modified based on the ΔH_{ds} of UO_2 measured in this work (see supporting information for further details regarding the calculations). ΔH_{ds} of $(U_yZr_{1-y})C_xO_z$ and ZrC were measured assuming a small amount of oxygen present in the samples that were explicitly included in calculating the thermochemical cycles. The oxidation enthalpies (ΔH_{ox}) of U, Zr, and C at 298 K, and the enthalpies associated with heating O_2 and CO_2 from 298 K to 1073 K, were calculated using FactSage software 8.3 [21] with the FactPS database, which contains data from [22–24], and are presented in Table 5. The enthalpies given in Tables 4 and 5, together with the stoichiometric coefficients in Table 2, were used in the thermochemical cycles shown in Tables 6 and 7 to calculate the formation enthalpies (ΔH_f) and ΔH_{ox} of the $(U_yZr_{1-y})C_xO_z$ samples shown in Table 8 along with ΔH_f and ΔH_{ox} of ZrC measured in this study. The ΔH_{ox} of ZrC measured in this work (–1315.58±7.36 kJ·mol^{-1}) is slightly more negative (~7.5 kJ.mol^{-1}) than the value (–1294.34±6.47 kJ·mol^{-1}) calculated using FactSage software with the FactPS and FToxid databases [21,22,24]. The measured ZrC formation enthalpy (–170.87±21.80 kJ·mol^{-1}) fall within the previously reported range (172 to 222 kJ·mol^{-1}) [27,28]. The UC formation and oxidation enthalpies obtained in this work (–101.4±21.6 kJ·mol^{-1} and –1523.2±21.6 kJ·mol^{-1}, respectively) are consistent, within experimental error, with the earlier measurements from Goncharov et al. [17]. Calculation details for ZrC and UC enthalpies are given in the supporting information. The enthalpies of drop solution of the $(U_yZr_{1-y})C_xO_z$ solid solutions and the UC and ZrC end members from Table 4 were used to calculate enthalpies of mixing of the solid solutions given in Table 9 using Eq. (2):

$$\Delta H_{mix} = -\Delta H_{ds}[(U_yZr_{1-y})C_xO_z)] + y\Delta H_{ds}(UC) + (1-y)\Delta H_{ds}(ZrC). \quad (2)$$

The drop solution enthalpies of the $(U_yZr_{1-y})C_xO_z$ solid solutions are plotted as a function of uranium content in Fig. 6. The curve (excluding one outlier, see below) were fitted by a quadratic function (Eq. (3)), which indicates thermodynamically non-ideal solid solution behavior as uranium content increases:

$$\Delta H_{ds} = a + bx + cx^2. \quad (3)$$

where a = –649.71±1.73 kJ·mol^{-1}·atom^{-1}, b = –172.76±32.55 kJ·mol^{-1}·atom^{-1}, and c = 80.02±32.52 kJ·mol^{-1}·atom^{-1}, with an adjusted R^2 = 0.9919. The data point for $U_{0.3}Zr_{0.7}C_{0.98}O_{0.068}$ sample (blue sphere in Fig. 6) was excluded from the fit because of its much higher oxygen content than the other samples. The higher oxygen content in the $U_{0.3}Zr_{0.7}C_{0.98}O_{0.068}$ sample reduces the heat released during the reaction with the solvent, which results in a less exothermic drop solution enthalpy.

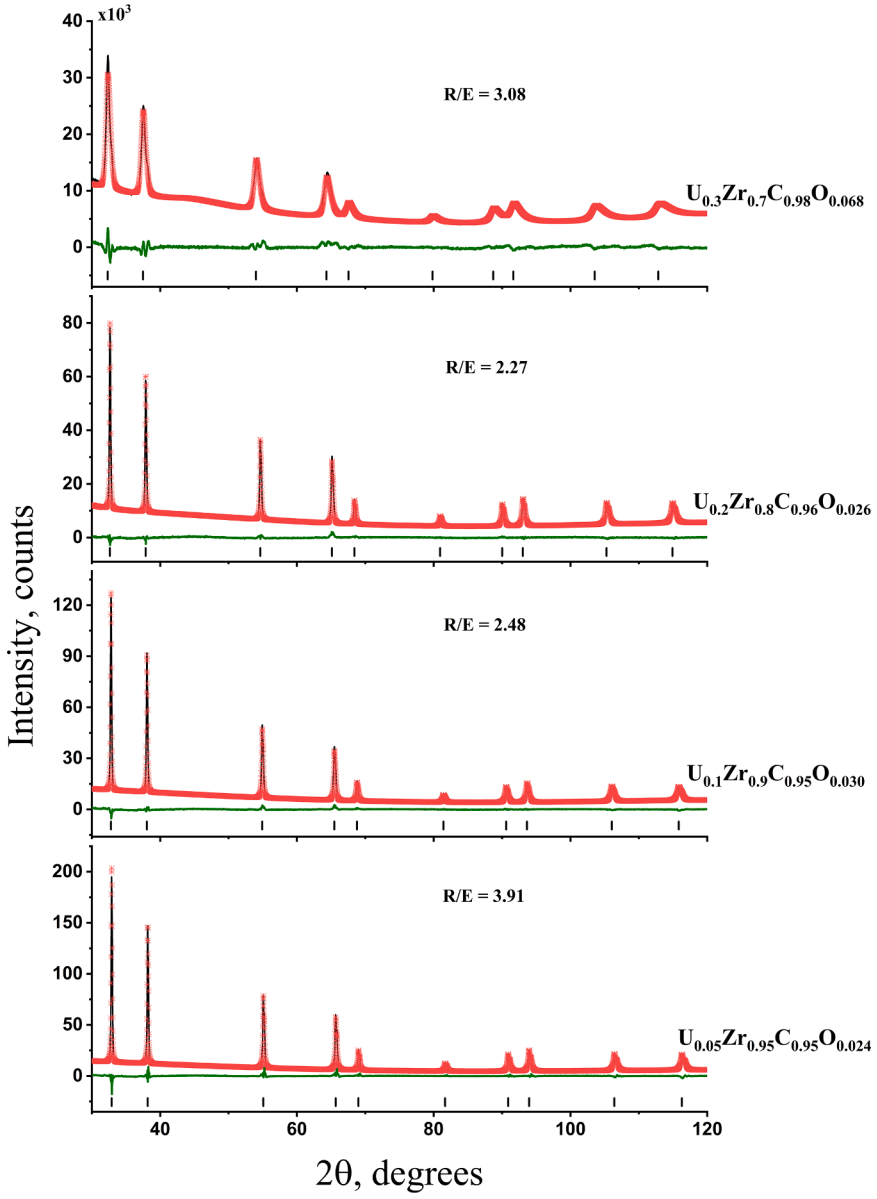

Fig. 4. X-ray diffraction patterns of the $(U_yZr_{1-y})C_xO_z$ samples. Black pattern – measured data. Red asterisks – calculated pattern. Olive pattern represents difference between measured and calculated patterns. Thick marks - allowed reflection positions. Goodness of fit R/E in which R and E are weighted and expected values, respectively.

Table 3
Unit-cell dimensions of the $(U_yZr_{1-y})C_xO_z$ samples.

Sample ID	a = b = c (Å)†	Volume (Å^3)
ZrC	4.69449(2)	103.458(1)
$U_{0.05}Zr_{0.95}C_{0.95}O_{0.024}$	4.712244(7)	104.649(3)
$U_{0.1}Zr_{0.9}C_{0.95}O_{0.030}$	4.72364(8)	105.397(3)
$U_{0.2}Zr_{0.8}C_{0.96}O_{0.026}$	4.74812(8)	107.044(3)
$U_{0.3}Zr_{0.7}C_{0.98}O_{0.068}$	4.8055(6)	110.98(2)
UC*	4.9648(1)	122.379(4)

†Uncertainties of the contents are given in parentheses.
$(U_yZr_{1-y})C_xO_z$ – PDF card: 04–020–5318. α=β=γ=90°,
and ZrC – PDF card: 04–003–7140.
*From [14].

A similar fitting approach was applied in the subsequent analyses.

The dependence of the mixing enthalpies of $(U_yZr_{1-y})C_xO_z$ on uranium content is presented in Fig. 7. The mixing enthalpies of the solid solution are positive, indicating thermodynamic instability if they exceed the negative contribution from the mixing entropy. The datapoints in Fig. 7 can be fitted by assuming a regular solution model using the quadratic polynomial Eq. (4):

$$\Delta H_{mix} = x(1-x)\Omega. \quad (4)$$

where Ω is the regular solution parameter for the cubic phase. The regular solution parameter is obtained from the quadratic term ($c = 80.02 \pm 32.52$ kJ·mol^{-1}·atom^{-1}) in Eq. (3). The quadratic fit is shown as dashed lines in Fig. 7. The high positive value of Ω indicates potential phase separation from destabilizing the solid solution.

Fig. 8 shows the formation enthalpies of the $(U_yZr_{1-y})C_xO_z$ solid solutions as a function of uranium content. The formation enthalpies of the solid solutions become less exothermic with increasing uranium content, suggesting that the solid solutions are energetically less favorable compared with their end members.

Fig. 9 shows the variation of the $(U_yZr_{1-y})C_xO_z$ oxidation enthalpies with increasing uranium content. The enthalpies of oxidation become more exothermic as uranium content increases.

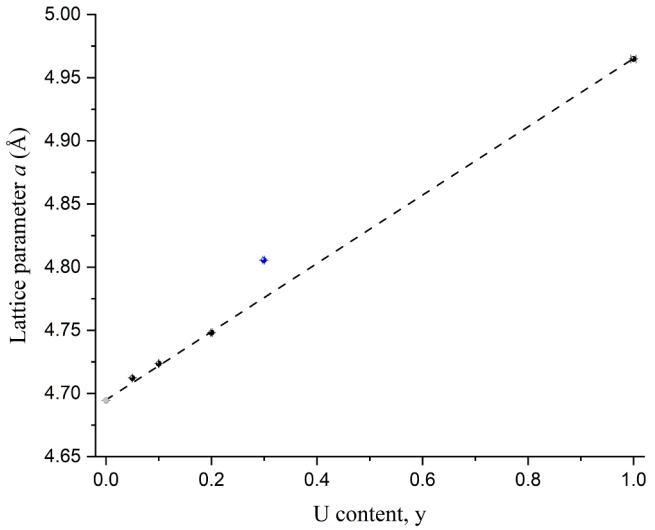

Fig. 5. Unit cell parameter a of $(U_yZr_{1-y})C_xO_z$ samples versus uranium content, y. Blue sphere represents $U_{0.3}Zr_{0.7}C_{0.98}O_{0.068}$ sample datapoint excluded from fitting. Gray circle represents UC datapoint from reference [14].

Table 4
Drop solution enthalpies (ΔH_{ds}) of $(U_yZr_{1-y})C_xO_z$ samples, UO_3, ZrO_2, UC, and ZrC in sodium molybdate solvent at 1073 K.

Sample	ΔH_{ds} (kJ·mol^{-1})*	ΔH_{ds} (kJ·mol^{-1}·atom^{-1})
ZrO_2	29.20±1.60 [18,19]	9.73±0.53
UO_3	27.90±0.80 [20]	6.98±0.20
ZrC	–1299.56±6.69 (8)	–649.78±3.35
UC	–1484.98±22.09†	–742.49±11.05
$U_{0.05}Zr_{0.95}C_{0.95}O_{0.024}$	–1248.27±22.26 (10)	–651.91±11.52
$U_{0.1}Zr_{0.9}C_{0.95}O_{0.030}$	–1324.23±14.75 (7)	–669.82±7.78
$U_{0.2}Zr_{0.8}C_{0.96}O_{0.026}$	–1344.54±22.63 (6)	–678.38±11.62
$U_{0.3}Zr_{0.7}C_{0.98}O_{0.068}$	–1357.74±17.91 (8)	–662.31±9.45

*Uncertainties are calculated as two standard deviations of the mean. Extra digits are retained to prevent round-off error. Number of experiments is given in parentheses. † UC drop solution enthalpy at 1073 K was calculated from that measured by Goncharov et al. [17] at 973 K. Calculation details of UC drop solution enthalpies are given in Tables S2 and S3 in the supporting information.

Table 5
Enthalpies associated with heat pick up of O2 and CO2 from room temperature to 1073 K and oxidation enthalpies of U, Zr, and C at 298 K.

Transition	ΔH (kJ·mol^{-1})*
O_2(g), 298 K → O_2(g), 1073 K	25.27±0.13
CO_2(g), 298 K → CO_2(g), 1073 K	37.40±0.19
U(s) + 1.5O_2(g) → UO_3(s)	–1222.98±6.11
Zr(s) + O_2(g) → ZrO_2(s)	–1100.80±5.50
C(s) + O_2(g) → CO_2(s)	–393.52±1.97

* Uncertainties are assumed to be 0.5% error in the enthalpy. Extra digits are retained to prevent round-off error.

4. Discussion

The enthalpies of drop solution, mixing, and formation of the uranium-zirconium carbide solid solutions, relative to their UC and ZrC end members, indicate a positive deviation from ideality with a tendency towards exsolution. This suggests that the UC-ZrC solid solutions with lower enthalpic stabilities may decompose to their end members at high temperatures in a space nuclear reactor. However, the variation of the unit cell parameter *a* with uranium content follows Vegard's law and shows no deviation from linearity, except for the $U_{0.3}Zr_{0.7}C_{0.98}O_{0.068}$ composition, which contains higher oxygen content (Table 2). This suggests that the thermodynamic non-ideality of the $(U_yZr_{1-y})C_xO_z$ solid solution arises not from the volumetric mismatch between U and Zr in the cationic sublattice, but rather from differences in chemical bonding [29].

Our results also suggest that the higher oxygen content in the $U_{0.3}Zr_{0.7}C_{0.98}O_{0.068}$ sample was enough to cause ionic substitution in the crystalline structure of the solid solution, resulting in a deviation from

Table 6
Thermochemical cycle for calculating formation and oxidation enthalpies of $(U_yZr_{1-y})C_xO_z$ samples at 298 K.

$(U_yZr_{1-y})C_xO_z$ (s, 298 K) + [1.5y + (1 – y) + x – z/2] O_2(g, 1073 K) → yUO_3(sln, 1073 K) + (1 – y) ZrO_2(sln, 1073 K) + xCO_2(g1073 K)	$\Delta H_1 = \Delta H_{ds}$, $(U_yZr_{1-y})C_xO_z$
[1.5y + (1 – y) + x – z/2]O_2(g, 298 K) → [1.5y + (1 – y)+ x – z/2]O_2(g, 1073 K)	ΔH_2 = [1.5y + (1 – y) + x – z/2]$\Delta H_{(298–1073\ K)}$, O_2
xCO_2(g, 298 K) → xCO_2(g, 1073 K)	$\Delta H_3 = -x\Delta H_{(298–1073\ K)}$, CO_2
yUO_3(s, 298 K) → yUO_3(sln, 1073 K)	$\Delta H_4 = -y\Delta H_{ds}$, UO_3
(1 – y)ZrO_2(s, 298 K) → (1 – y)ZrO_2(sln, 1073 K)	$\Delta H_5 = -(1-y)\Delta H_{ds}$, m-$ZrO_2$
$(U_yZr_{1-y})C_xO_z$(s, 298 K) + [1.5y + (1 – y) + x – z/2] O_2(g, 298 K) → yUO_3(s, 298 K) + (1 – y)ZrO_2(s, 298 K) + xCO_2(g, 298 K)	ΔH_6* = ΔH_{ox}, $(U_yZr_{1-y})C_xO_z$

*$\Delta H_6 = \Delta H_1 + \Delta H_2 + \Delta H_3 + \Delta H_4 + \Delta H_5$

Table 7
Thermochemical cycle for calculating formation enthalpies of $(U_yZr_{1-y})C_xO_z$ samples at 298 K.

$(U_yZr_{1-y})C_xO_{z(s,\ 298\ K)}$ + (1.5y + 1 – y + x – z/2)$O_{2(g,\ 298\ K)}$ → $yUO_{3(s,\ 298\ K)}$ + (1 – y)$ZrO_{2(s,\ 298\ K)}$ + $xCO_{2(g,\ 298\ K)}$	ΔH_6= –ΔH_{ox}, $(U_yZr_{1-y})C_xO_z$
$yU_{(s,\ 298\ K)}$ + 1.5$yO_{2(g,\ 298\ K)}$ → $yUO_{3(s,\ 298\ K)}$	$\Delta H_7 = y\Delta H_{ox}$, U-$UO_3$
(1 – y)$Zr_{(s,\ 298\ K)}$ + (1 – y)$O_{2(g,\ 298\ K)}$ → (1 – y)$ZrO_{2(s,\ 298\ K)}$	$\Delta H_8 = (1-y)\Delta H_{ox}$, Zr-$ZrO_2$
$xC_{(s,\ 298\ K)}$ + $xO_{2(g,\ 298\ K)}$ → $xCO_{2(s,\ 298\ K)}$	$\Delta H_9 = x\Delta H_{ox}$, C-$CO_2$
$yU_{(s,\ 298\ K)}$ + (1 – y)$Zr_{(s,\ 298\ K)}$ + $xC_{(s,\ 298\ K)}$ + z/2$O_{2(g,\ 298\ K)}$ → $(U_yZr_{1-y})C_xO_{z(s,\ 298\ K)}$	ΔH_{10}†= ΔH_f, $(U_yZr_{1-y})C_xO_{z,(s,\ 298\ K)}$

†$\Delta H_{10} = \Delta H_6 + \Delta H_7 + \Delta H_8 + \Delta H_9$

Table 8
Enthalpies of formation (ΔH_f) and oxidation (ΔH_{ox}) of $(U_yZr_{1-y})C_xO_z$ samples at 298 K.

Sample ID	$\Delta H_{f,element}$ (kJ·mol^{-1})*	$\Delta H_{f,element}$ (kJ·mol^{-1}·atom^{-1})*	ΔH_{ox} (kJ·mol^{-1})*	ΔH_{ox} (kJ·mol^{-1}·atom^{-1})*
ZrC	–170.87 ±21.66	–85.43 ±10.83	–1315.58 ±6.93	–657.79 ±3.47
$U_{0.05}Zr_{0.95}C_{0.95}O_{0.024}$	–179.90 ±23.66	–91.32 ±12.01	–1299.28 ±22.32	–659.53 ±11.55
$U_{0.1}Zr_{0.9}C_{0.95}O_{0.030}$	–147.05 ±16.63	–74.38 ±8.42	–1338.63 ±14.83	–677.10 ±7.83
$U_{0.2}Zr_{0.8}C_{0.96}O_{0.026}$	–143.83 ±23.72	–72.57 ±11.97	–1357.61 ±22.67	–684.97 ±11.64
$U_{0.3}Zr_{0.7}C_{0.98}O_{0.068}$	–153.49 ±19.15	–74.88 ±9.34	–1370.27 ±17.96	–668.43 ±8.99
UC	–132.39 ±23.02	–66.20 ±11.51	–1484.11 ±22.11	–742.06 ±11.06

*Extra digits are retained to prevent round-off error.

Table 9
Enthalpies of mixing of the $(U_yZr_{1-y})C_xO_z$ samples at 298 K.

Sample ID	ΔH_{mix} (kJ·mol^{-1}·atom^{-1})*
ZrC	0.00±6.9
$U_{0.05}Zr_{0.95}C_{0.95}O_{0.024}$	–2.51±12.36
$U_{0.1}Zr_{0.9}C_{0.95}O_{0.030}$	10.77±8.92
$U_{0.2}Zr_{0.8}C_{0.96}O_{0.026}$	10.06±12.42
$U_{0.3}Zr_{0.7}C_{0.98}O_{0.068}$	–15.19±10.59
UC	0.00±10.65

*Extra digits are retained to prevent round-off error.

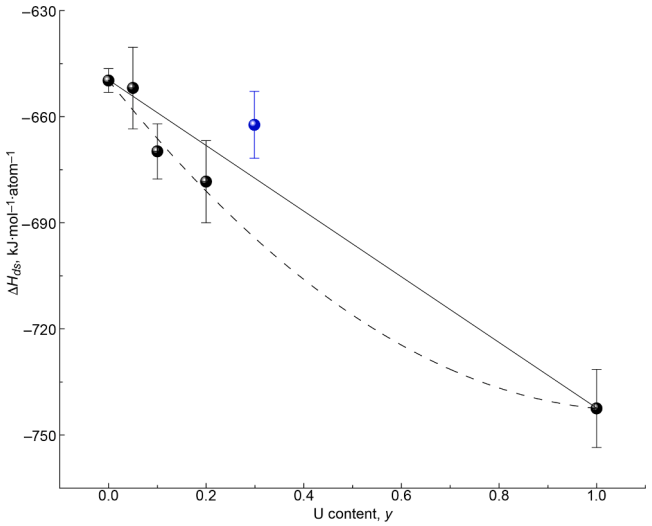

Fig. 6. Drop solution enthalpies of $(U_yZr_{1-y})C_xO_z$ solid solutions versus uranium content fitted by quadratic equation (Eq. (3)). Blue sphere represents $U_{0.3}Zr_{0.7}C_{0.98}O_{0.068}$ sample datapoint excluded from fitting.

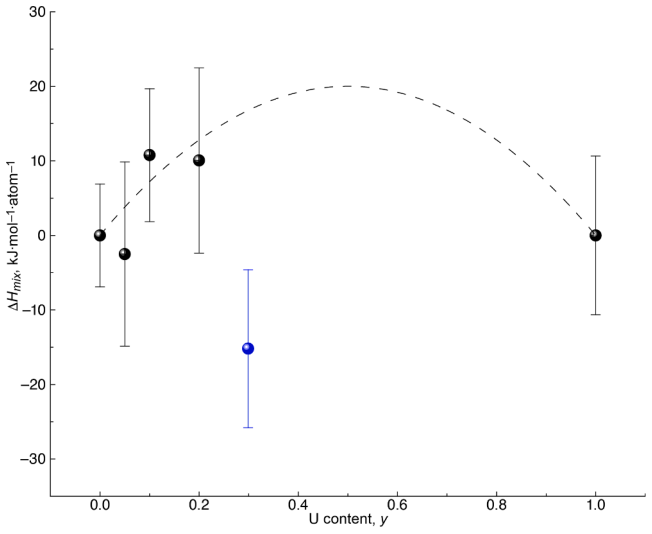

Fig. 7. Enthalpies of mixing of $(U_yZr_{1-y})C_xO_z$ solid solutions versus uranium content fitted by quadratic equation (Eq. (4)). Blue sphere represents $U_{0.3}Zr_{0.7}C_{0.98}O_{0.068}$ sample datapoint excluded from fitting.

the linear dependence of the lattice parameter as a function of the U concentration. The higher oxygen content in the $U_{0.3}Zr_{0.7}C_{0.98}O_{0.068}$ sample also accounts for its reduced exothermicity observed in drop solution calorimetric measurements (Fig. 6), its improved thermodynamic stability as reflected by its more negative enthalpies of mixing and formation (Figs. 7 and 8, respectively), and its enhanced oxidation resistance (less exothermic oxidation enthalpy, Fig. 9). The stabilizing role of oxygen in the UC-ZrC solid solution is consistent with prior discussions of thermodynamic stability of crystalline silicon carbide polymer-derived ceramic fibers [30] and nanodiamonds with oxygen containing functional groups [31]. Finally, the increasingly positive formation enthalpies observed with higher uranium content (Fig. 8) further indicate a reduction in thermodynamic stability as the smaller octahedrally coordinated Zr^{4+} cation (0.72 Å as ionic radius) is substituted by the larger U^{4+} cation (0.89 Å). Ionic radii of U^{4+} and Zr^{4+} are taken from the Shannon table [32], considering a coordination number of 6.

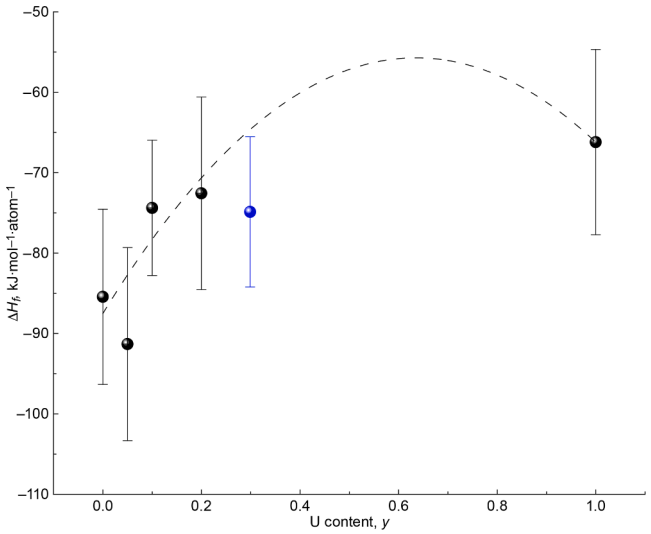

Fig. 8. Enthalpies of formation of $(U_yZr_{1-y})C_xO_z$ solid solutions versus uranium content fitted by quadratic equation $\Delta H_f = -87.52\pm5.59$ kJ·mol^{-1}·atom^{-1} + [(100.16±60.02 kJ·mol^{-1}·atom^{-1})·y] + [(−78.85±56.33 kJ·mol^{-1}·atom^{-1})·y^2]. Blue sphere represents $U_{0.3}Zr_{0.7}C_{0.98}O_{0.068}$ sample datapoint excluded from fitting.

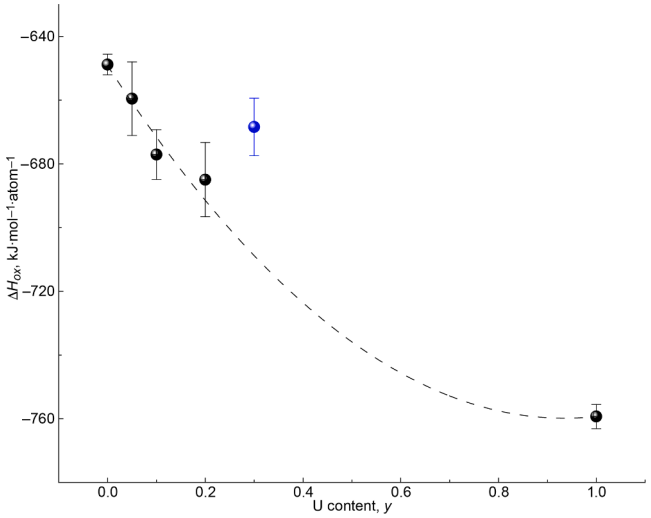

Fig. 9. Enthalpies of oxidation of $(U_yZr_{1-y})C_xO_z$ solid solutions versus uranium content fitted by quadratic equation $\Delta H_{ox} = -649.20\pm2.04$ kJ·mol^{-1}·atom^{-1} + [(−236.67±39.27 kJ·mol^{-1}·atom^{-1})· y] + [(126.57±38.50 kJ·mol^{-1}·atom^{-1})·y^2]. Blue sphere represents $U_{0.3}Zr_{0.7}C_{0.98}O_{0.068}$ sample datapoint excluded from fitting.

5. Conclusions

The formation, oxidation, and mixing enthalpies of uranium-zirconium carbide solid solutions hypostoichiometric in carbon were measured by high-temperature drop solution calorimetry. The $(U_yZr_{1-y})C_x$ solid solutions are energetically less stable than their corresponding physical mixtures of UC and ZrC end members. Although this reflects an enthalpic tendency towards phase separation and changes in the crystal structure, the configurational and vibrational entropies of the solid solutions could be positive enough to make their Gibbs energies negative for energetic stabilization. The solid solutions become less stable and more reactive towards oxidation with increasing uranium content. In contrast, the incorporation of oxygen enhances the stability of the solid solutions and improves their resistance to oxidation. Oxygen incorporated in carbide solid solutions may be considered for the engineering of

future iterations of nuclear fuels. The results presented here provide a new benchmark dataset for CALPHAD modeling of the thermochemical stability of carbide-based nuclear fuels for space reactors.

CRediT authorship contribution statement

Gustavo Costa: Writing – review & editing, Writing – original draft, Resources, Project administration, Methodology, Investigation, Funding acquisition, Formal analysis, Data curation, Conceptualization. **Malina K. Slizik:** Resources. **Jason C. Reynolds:** Writing – review & editing, Writing – original draft, Resources, Methodology, Funding acquisition. **Scarlett Widgeon Paisner:** Writing – review & editing, Writing – original draft, Resources, Methodology, Investigation. **Joseph C. Schaeperkoetter:** Writing – review & editing, Writing – original draft, Resources, Methodology, Investigation, Formal analysis. **Erofili Kardoulaki:** Writing – review & editing, Writing – original draft, Resources, Methodology, Investigation, Formal analysis. **Shinhyo Bang:** Writing – review & editing, Writing – original draft, Methodology, Investigation, Formal analysis. **Xiaofeng Guo:** Writing – review & editing, Writing – original draft, Methodology, Investigation, Formal analysis. **Theodore M. Besmann:** Writing – review & editing, Writing – original draft.

Declaration of competing interest

The authors declare that they have no known competing financial interests or personal relationships that could have appeared to influence the work reported in this paper.

Acknowledgments

This work was supported by NASA's Space Technology Mission Directorate (STMD) through the Space Nuclear Propulsion (SNP) project. We also acknowledge the partial support from the United States Nuclear Regulatory Commission, Office of Nuclear Regulatory Research (RES) under award No. 31310023M0011, and the U.S. Department of Energy. Part of this work was performed at Los Alamos National Laboratory, which is operated by Triad National Security, LLC, for the National Nuclear Security Administration of the U.S. Department of Energy under contract number 89233218CNA000001.

Supplementary materials

Supplementary material associated with this article can be found, in the online version, at doi:10.1016/j.jnucmat.2026.156680.

Data availability

Data will be made available on request.

References

[1] S. Borowski, D. McCurdy, T. Packard, Nuclear thermal propulsion (NTP): a proven growth technology for human NEO/Mars exploration missions, in: Proc. IEEE Aerospace Conf, IEEE, Big Sky, Montana, 2012.
[2] L.L. Lyon, Performance of (U,Zr)C-graphite (composite) and of (U,Zr)C (carbide) fuel elements in the nuclear furnace 1 test reactor, Alamos Sci. Lab. (1973) 1–67.
[3] America at the Threshold, Report of the Synthesis Group On America's space Exploration Initiative. Superintendent of Documents, U.S. Government Printing Office, Washington, DC, 1991.
[4] E.K. Storms, J. Griffin, Thermodynamic and phase relationships of the zirconium-uranium-carbon system, High Temp. Sci. 5 (1973) 423–437.
[5] A. Lanin, Nuclear Rocket Engine Reactor, Springer, New York, 2012.
[6] D. Farr, M. Bowman, Thermodynamic properties and phase relationships in the U-C system and selected U-M-C systems, Alamos Natl. Lab. Rep. (1963). LADC-5907.
[7] D.P. Butt, T.C. Wallace Sr, The U-Zr-C ternary phase diagram above 2473 K, J. Am. Ceram. Soc. 76 (1993) 1409–1419.
[8] L.D. Brownlee, The pseudo-binary systems of uranium carbide with zirconium carbide, tantalum carbide, and niobium carbide, J. Inst. Met. 87 (1958) 58–61.
[9] B. Panda, R.R. Hickman, S. Shah, Solid solution carbides are the key fuels for future nuclear thermal propulsion. Joint Army-Navy-NASA-Air Force (JANNAF) Meeting, Monterey, CA (2005).
[10] E. Kardoulaki, J.T. White, J.K.P. Williams, et al., Synthesis, thermal conductivity, and hydrogen compatibility of a high melt point solid solution uranium carbide, (U0.2Zr0.8)C, Nucl. Mater. Energy 33 (2022) 101290.
[11] J.C. Schaeperkoetter, S.W. Paisner, A. Gonzales, et al., Impact of composition on the thermophysical properties of (U,Zr)C solid solution carbide fuels, J. Nucl. Mater. 607 (2025) 155669.
[12] J.O. Andersson, T. Helander, L. Höglund, et al., Thermo-Calc & DICTRA, computational tools for materials science, Calphad 26 (2002) 273–312.
[13] C. Guéneau, N. Dupin, L. Kjellqvist, et al., TAF-ID: an international thermodynamic database for nuclear fuels applications, Calphad 72 (2021) 102212.
[14] E. Kardoulaki, M. Kosmidou, J. Rizk, et al., Assessment of the hydrogen resistance of $(U_{0.2}Zr_{0.8})C$ following exposure up to 2600 K, Ceram. Int. 51 (2025) 20482–20491.
[15] C. Ang, Properties of solid-solution uranium zirconium carbides for high temperature nuclear applications, J. Nucl. Mater. 615 (2025) 155929.
[16] E.C. Kindall, N.S. Yaw, M.C.D. Wilkins, et al., Thermal oxidation and high temperature structural behavior of uranium carbide, Npj. Mater. Degrad. 10 (2026) 1–10.
[17] V.G. Goncharov, J. Liu, A. Strzelecki, et al., Energetics of oxidation and formation of uranium monocarbide, J. Nucl. Mater. 581 (2023) 154446.
[18] A. Navrotsky, Progress and new directions in high temperature calorimetry revisited, Phys. Chem. Min. 24 (1997) 222–241.
[19] A. Navrotsky, Progress and new directions in calorimetry: a 2014 perspective, J. Am. Ceram. Soc. 97 (2014), 3949-3359.
[20] M. Scharrer, L. Bonatti, T. Geraci, et al., The joys and jitters of high-temperature calorimetry, J. Am. Ceram. Soc. 97 (2024) 1–36.
[21] C.W. Bale, E. Bélisle, P. Chartrand, et al., FactSage thermochemical software and databases, 2010-2016, CALPHAD 54 (2016) 35–53.
[22] D.R. Stull and H. Prophet, JANAF thermochemical tables. U.S. Department of commerce, Washington (1985).
[23] E.H.P Cordfunke, R.J.M. Konings, Thermochemical data for reactor materials and fission products, N. Holl. Amst. (1990).
[24] I. Barin, Thermochemical Data of Pure Substances, 3rd edition, VCH Verlag GmbH. Weinheim, Germany, 1995.
[25] D.L. Drey, E.C. O'Quinn, T. Subramani, et al., Disorder in $Ho_2Ti_{2-x}Zr_xO_7$: pyrochlore to defect fluorite solid solution series, R. Soc. Chem. Adv. 10 (2020) 34632.
[26] X. Guo, Thermodynamics of Material Containing actinides: Garnets, Metal uranates, and Uranyl Peroxide, University of California, Davis, 2014.
[27] I.L. Shabalin, Ultra-high Temperature Materials II, Refractory Carbides I (Ta, Hf, Nb and Zr Carbides), Springer, 2019.
[28] S.V. Ushakov, A. Navrotsky, Q.J. Hong, et al., Carbides and nitrides of zirconium and hafnium, Materials 17 (2019) 2728.
[29] A.C. Strzelecki, M.X. Zhao, W. Yu, et al., Crystal chemistry and thermodynamics of HREE (Er, Yb) mixing in a xenotime solid solution, ACS. Earth. Space Chem. 6 (2022) 1375–1389.
[30] G.J. Leonel, S.B. Mujib, G. Singh, A. Navrotsky, Thermodynamic stabilization of crystalline silicon carbide polymer-derived ceramic fibers, Int. J. Ceram. Eng. Sci. 4 (2022) 315–326.
[31] G.C.C. Costa, O. Shenderova, V. Mochalin, et al., Thermochemistry of nanodiamond terminated by oxygen containing functional groups, Carbon. N. Y. 80 (2014) 544–550.
[32] R.D. Shannon, Revised effective ionic radii and systematic studies of interatomic distances in halides and chalcogenides, Acta Crystallogr. (1976) 751–767. A32.